Biological Trace Element Research (2021) 199:1802–1811
https://doi.org/10.1007/s12011-020-02309-2

Osteogenesis Promotion of Selenium-Doped Hydroxyapatite for Application as Bone Scaffold

Solmaz Zakhireh[1,2] · Khosro Adibkia[3] · Younes Beygi-Khosrowshahi[4] · Mohammad Barzegar-Jalali[5]

Received: 8 May 2020 / Accepted: 24 July 2020 / Published online: 20 August 2020

Abstract

The combined bioceramic of selenium (Se) and hydroxyapatite (HA) has been considered as a moderate bone scaffold biomaterial. In the present work, Se was doped into the HA structure using the mechano-chemical alloying (MCA) method for the improvement of osteogenic properties of HA. HA extracted from fish bone and Se-doped hydroxyapatite (Se-HA) were analyzed using X-ray diffraction spectra (XRD), scanning electron microscope (SEM), energy dispersion X-ray spectrometer (EDX), and Fourier transform infrared spectroscopy (FT-IR). In-vitro cell responses on the Se-HA bioceramic scaffold were investigated using human adipose-derived mesenchymal stem cells (hAD-MSCs). The effect of Se on cell proliferation was studied by MTT assay, and cell adhesion responses were analyzed by optical microscopy and SEM. Furthermore, the effect of Se on osteogenic properties of HA was studied by alkaline phosphatase (ALP) activity, alizarin red S (ARS) staining, and Western blot tests. The MTT results showed that the Se dopant synergistically increases the proliferation of hAD-MSCs. Moreover, good cell-adhesive and osteoblast-shaped behaviors were observed on the Se-HA scaffold. The results of osteogenic differentiation demonstrated synergistically enhanced ALP activity and calcification on the Se dopant compared to HA. Also, the results of Western blot test presented that the differentiation of hAD-MSCs toward being a bone tissue was increased by up to 50% while selenium doping. Additional MTT analysis using Human Bone Osteosarcoma cell line (KHOS-240S) revealed the antiproliferative activity of the Se-HA scaffold against bone cancerous cells. Therefore, it has been concluded that Se-HA bioceramic can be employed as a scaffold with simultaneous anticancer and bone regenerative properties.

Keyword Hydroxyapatite · Selenium · Mechano-chemical · Osteogenesis

Introduction

Hydroxyapatite (HA) bioceramic, with the chemical formula of $Ca_{10}(PO4)_6(OH)_2$, has gained special importance in the biomedical engineering owing to its biocompatibility and bioactivity. Furthermore, chemical and structural similarities to the bone, as well as osteoconductive properties, have led to the use of HA as a bone scaffold in tissue engineering and regenerative medicine [1–3]. For more improvements of the biomedical properties of HA, several dopants such as magnesium [4], strontium [5], silicon [6], potassium [7], and lithium [8] have been applied. Some dopants like zinc [9], silver [10], and copper [11] enhanced the osteogenesis as well as antibacterial properties. Selenium (Se) is a widely used mineral in bone regeneration applications. It could exert antibacterial activity in HA due to its ability to produce hydrogen peroxide (H_2O_2) and superoxide ($O_2^{\bullet -}$) [12, 13]. It is also known to induce anticancer effects by modulating apoptotic gene expression [13, 14].

To dope elements into the HA structure, several different methods including hydrothermal treatment [15], co-precipitation [16], microwave [17], and sol-gel [18] have been applied. The Mechano-chemical alloying method is an interesting technique to be used for alloying of HA due to its simplicity, cheapness, and vast area of applications [19, 20].

✉ Mohammad Barzegar-Jalali
barzegarjalali@tbzmed.ac.ir

1 Drug Applied Research Center, Tabriz University of Medical Sciences, Tabriz, Iran

2 Student Research Committee, Tabriz University of Medical Sciences, Tabriz, Iran

3 Research Center for Pharmaceutical Nanotechnology and Faculty of Pharmacy, Tabriz University of Medical Sciences, Tabriz, Iran

4 Chemical Engineering Department, Faculty of Engineering, Azarbaijan Shahid Madani University, Tabriz, Iran

5 Pharmaceutical Analysis Research Center and Faculty of Pharmacy, Tabriz University of Medical Sciences, Tabriz, Iran

Following the previous studies related to antibacterial and anticancer properties of Se in HA structure, in the present work, the effect of Se on the osteogenesis properties of HA was investigated using human adipose-derived mesenchymal stem cells (hAD-MSCs). In this regard, Se-doped hydroxyapatite (Se-HA) was prepared using the mechano-chemical alloying process. Then, in vitro cell behavior analysis was performed using MTT assay, optical microscopy, scanning electron microscopy (SEM), alkaline phosphatase (ALP) activity, alizarin red S (ARS) staining, and Western blot tests to consider synergistic effect of Se-HA scaffold.

Materials and Methods

Materials

Human adipose-derived mesenchymal stem cells were received from the Iranian Biological Resource Center (Tehran, Iran). Selenium dioxide (SeO_2) powder, Trypan blue solution, and MTT salt were purchased from Sigma-Aldrich (St. Louis, MO, USA). All cell culture components were obtained from Gibco (Life Technologies Ltd., UK). Other chemicals were acquired from Merck (Kenilworth, NJ, USA).

Preparation of Hydroxyapatite

HA powder was prepared using natural source of fish bone. The bone structure of white fish was put into the boiling water for 1 h following by heat treatment at 700 °C in air atmosphere for 2 h. To make suitable powder from the obtained HA, ball mill technique was employed. Polyethylene cups and zirconia balls (W% ball/powder = 10 to 1) were used in a ball mill with the speed of 200 rpm for 2 h.

Preparation of Selenium-Doped Hydroxyapatite

For doping Se into the HA matrix, SeO_2 powder with the molar ratio of 1:1 was combined with HA powder and put into planetary ball mill PM 400-RETSCH for the mechanical alloying procedure. Furthermore, a HA sample was treated the same for comparing with the Se-doped HA. The ball milling procedure was done at 300 rpm speed for 20 h with the ball to powder ratio of 1:10. This procedure was done using Tungsten carbide cups and balls. HA and Se-HA samples were heat-treated at 800 °C for 2 h in the air.

Characterization

X-ray Diffraction Spectra (XRD)

The phase analysis of samples was done using XRD (Advance D8, Bruker, Germany) with the incident radiation of Cu Kα (λ = 1.5406 Å). The scattering angle (2θ) range was selected between 20 and 60°, and the scan rate was 4°/min.

Scanning Electron Microscopy with Energy Dispersive X-ray Analysis (SEM-EDX)

The morphology and particle size of powders were studied using SEM-EDX (Philips, CM 20, Netherland). Before the specimens are attached to the SEM sample stub, they were coated by a thin conductive layer of Au. The beam voltage of 20 kV was applied for photographing.

For further investigation, the analytical technique of EDX was used to explore the chemical composition of the samples.

Fourier Transform Infrared Spectroscopy (FT-IR)

FTIR spectrometer (4600 unicam, JASCO, Tokyo, Japan) was benefitted to identify functional groups that exist in the samples. The wavenumber range of 400 to 4000 cm^{-1} was selected to measure mid-infrared light absorption. The samples were mixed with KBr (spectroscopic grade) as an IR-transparent carrier.

Cell Culture

Initially, disk-shaped samples with a diameter of 1 cm and thickness of 2 mm were produced using the compression technique. After sterilizing with autoclave in 200 °C, the samples were finalized for the cell culture media. Three culture media including control media and media accompanied by disk-like HA and Se-HA samples were prepared. The initial cell density of 2.5×10^5 cells/wall was seeded in a culture plate containing Dulbecco's modified eagle medium (DMEM) supplemented with 10% fetal bovine serum (FBS) and 1% penicillin-streptomycin. At last, the culture media were incubated at 37 °C in a humidified atmosphere of 5% CO_2. Every 2 days, the media were replaced with a fresh one.

MTT Assay

MTT (3-(4,5-dimethylthiazol-2-yl)-2, 5-diphenyl tetrazolium bromide) assay (Jigma Inc., St. Louis, Mo) was done to evaluate the proliferation of hAD-MSCs and Human Bone Osteosarcoma cell line (KHOS-240S) in culture media. First, 5 mg/ml MTT solution was prepared through solving in phosphate-buffered saline (PBS). Then, 100 μl MTT solution was added to 900 μl of DMEM/F12 medium to thin. Following, 1 ml thinned solution of MTT was poured into the each sample of 24-well plates. After 2 h, the supernatants were removed, and 1 ml of the stabilized solution including 10% Triton x-100, 0.1 M HCl, and isopropanol was added to dissolve purple-colored formazan crystals and shivered for 10 min. Finally, 200 μl of the produced solution was examined

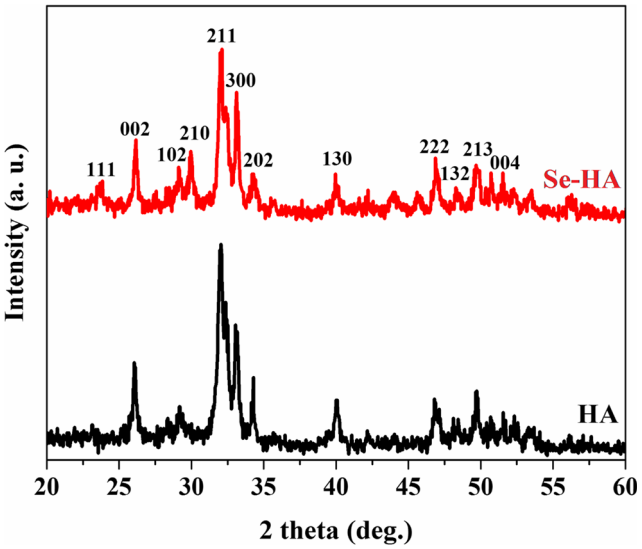

Fig. 1 XRD patterns of HA and Se-HA scaffolds

by microplate (Elx808, BioTek, USA) at a wavelength of 570 nm.

Cell Adhesion Analysis by Optical Microscopy and SEM

Optical microscopy (BioTek-1X832-Desk, USA) was employed to observe cell developments in culture media after 7 days. To see cell behavior on the surface of disk-like HA and Se-HA samples, the surface of samples was analyzed by SEM after 3 days. For this purpose, cell-cultured samples were washed with PBS, fixed by 4% formaldehyde solution at 4 °C, and finally rinsed with DI water.

Osteogenic Differentiation Analyses

For the evaluation of osteogenesis behavior of hAD-MSCs in HA and Se-HA culture media, suspensions containing HA and Se-HA powders were prepared in ethanol with a concentration of 10 gr/l. The well plate was coated using a doping procedure. After coating the bottom of the well plate, the samples were dried for 2 h at 120 °C in the oven. The osteogenic differentiation analyses were accomplished 7 days after cell culture.

Alkaline Phosphatase Activity

ALP is the most commonly used recognized marker of osteogenic differentiation. To assess the bone-forming activity of Se-HA scaffold, the ALP test was done after 3, 5, and 7 days according to the standard protocol of DGKC [21]. Briefly, the cells were washed using PBS, lysed by lysis buffer, incubated for 30 min at 37 °C, and kept overnight at 4 °C. Following, the

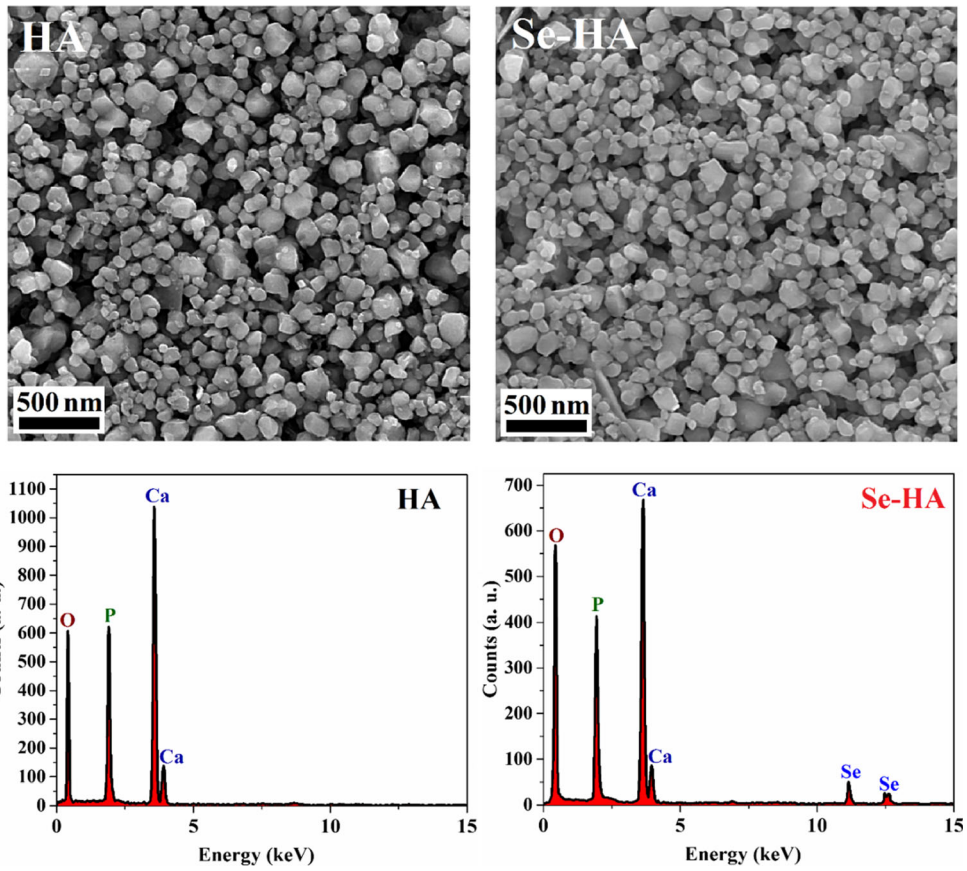

Fig. 2 SEM micrographs of HA and Se-HA scaffolds

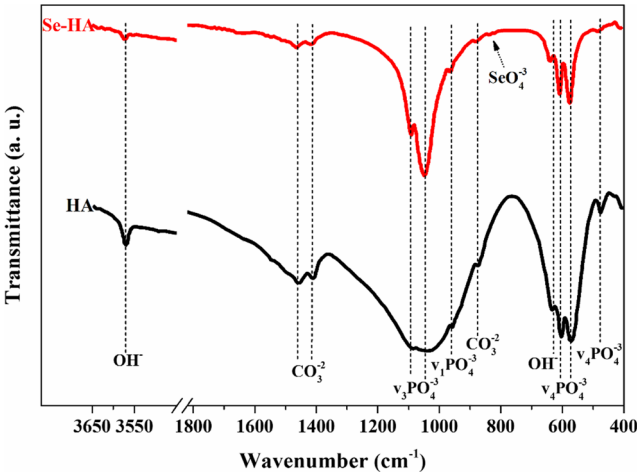

Fig. 3 FTIR spectra of HA and Se-HA scaffolds

resulting cells were collected into a tube and centrifuged for 10 min at 12,000 rpm. Then, the supernatant and p-nitrophenyl phosphate solution in a ratio of 1 to 20 were mixed in a 96-well plate and incubated in dark for 1 h at 25 °C. The ALP activity was measured using the fluorescence microscope system (Cytation 5, BioTek, USA) at a wavelength of 405 nm.

Alizarin Red S (ARS) Staining

ARS staining is used to identify calcium in the scaffold of tissue. The reaction is not strictly specific for calcium since manganese, magnesium, strontium, barium, and iron could interfere, but the quantities of these elements usually are not high enough to interfere with the ARS staining. ARS solution was prepared with dissolving 2 g ARS in 100 ml distilled water with adjusting pH to 4.1–4.3 with 10% ammonium hydroxide. The samples were deparaffinized using distilled water and then stained with the ARS solution for 2 min to produce nice red-orange staining of calcium. Finally, the stained samples were dehydrated in acetone and acetone-xylene (1:1) solution, respectively.

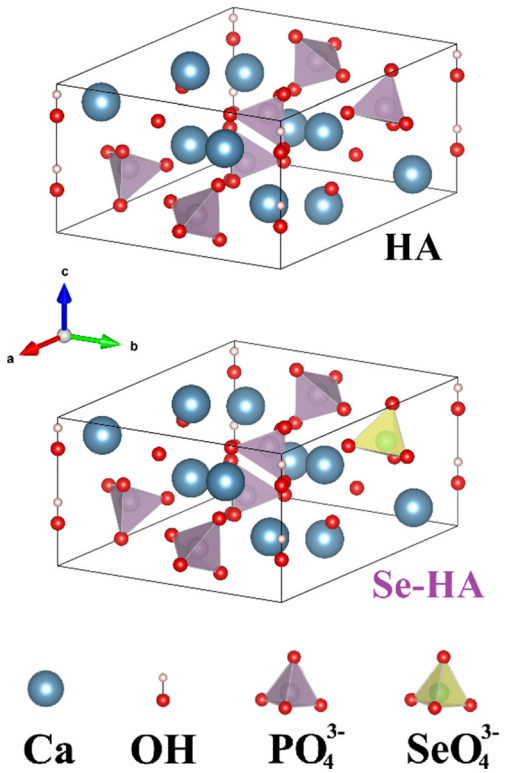

Fig. 4 3D structures of HA and Se-HA scaffolds

Western Blot Analysis

Western blotting is an important analytical technique used in molecular biology to detect specific proteins. To carry out this analysis, the cells were first washed twice with cold PBS solution and then lysed using lysis buffer containing Tris-HCL (500 μL, PH = 8), EDTA (0.003 g), NaCl (0.08 g), sodium deoxycholate (0.025 g), SDS (0.01 g), Triton (NP40 (1%)), and protease inhibitor cocktail. After centrifugation at 12000 rpm for 10 min, the protein solution was collected, and the protein concentration was measured by the Bradford protein assay protocol. The materials used in the Bradford method were Coomassie Blue G250 (5 mg), ethanol 95% (2 ml), phosphoric acid (5 mg), and distilled water up to 50 ml.

To have denaturation of protein, the amounts of total protein (20–50 μg) were boiled at 100 °C for 10 min. Molecular weight marker and equal amounts of protein were loaded into the wells of SDS-PAGE gel. The gel was run at 120 V for 45 min. The protein from the SDS-PAGE gel was transferred to the PVDF membranes using transferring buffer containing Tris (2.42 g), glycin (11.25 g), methanol (200 ml), and distilled water (100 ml). Then, the membrane was blocked for 45 min at room temperature with 5% skim milk which was diluted in the TBS–T solution containing Tris-HCL (20 ml), sodium chloride (8 g), Tween20 0.1 v/v (1 ml), and distilled water (100 ml). Afterward, the membranes were incubated with primary antibodies at 4 °C overnight and washed with TBS–T solution twice for 10 min. The prepared membranes were incubated with Anti-Rabbit antibody (1:1000) for 75 min at room temperature and washed with TBS–T solution for 15 min twice. The ECL advance reagent kit was used to detect the bands. Images were acquired by the exposure system.

Results and Discussion

XRD Characterization

The crystallinity and particle size of the prepared materials were analyzed by X-ray diffraction (XRD). Figure 1 displays XRD patterns of HA and Se-HA powder samples. The diffraction peaks showed hydroxyapatite with PDF Card no. JCP

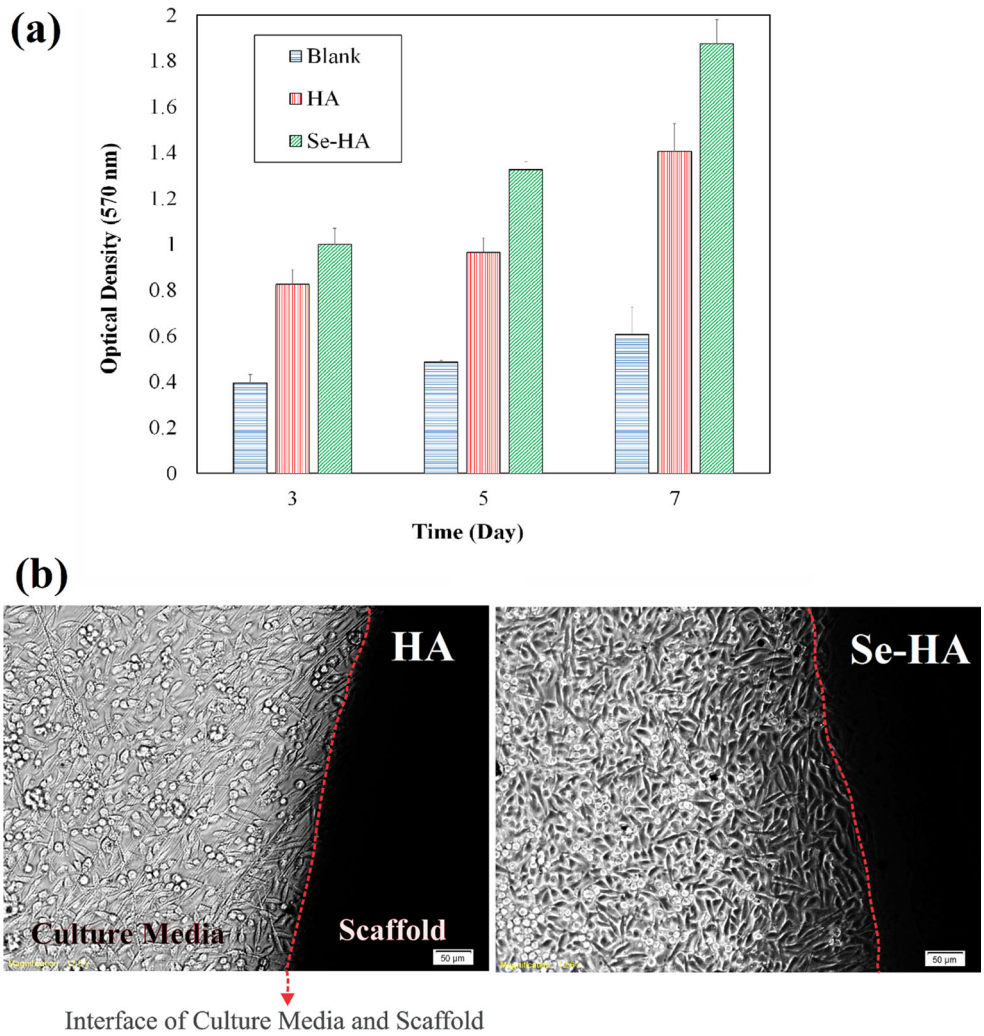

Fig. 5 **a** MTT test for hADMSCs in HA and Se-HA culture media on days 3, 5, and 7. **b** Optical microscopy images of culture media intersections with HA and Se-HA scaffolds on day 7

DS 09-432. According to the peaks related to HA and Se-HA samples, the crystallography structure was not changed by the doping of Se in HA structure. However, a small change was observed in the intensity of peaks. The average size of crystallites in HA and Se-HA samples were calculated using the Scherrer equation (Eq. 1) [22] as follows:

$$D = k\lambda/\beta\cos\theta \quad (1)$$

where, λ is the wavelength of X-ray (1.54 Angstrom), β is the width of peak in the half of maximum intensity, θ is the Brag angle in radian, and k is the Scherer constant (0.96). The sizes of crystallites calculated through Eq. (1) were obtained to be 87 and 78 nm for HA and Se-HA powders, respectively. Khan et al. [13] reported that the intensity of XRD peaks and the size of crystallites are decreased by doping Se in the HA matrix. The change in network constants of HA was due to the substitution of phosphor atoms by Se as well as the formation of strains in the matrix [23]. With increasing strain, crystal defects in the matrix are increased, leading to a decrease in crystallites size and peaks intensity [13, 23].

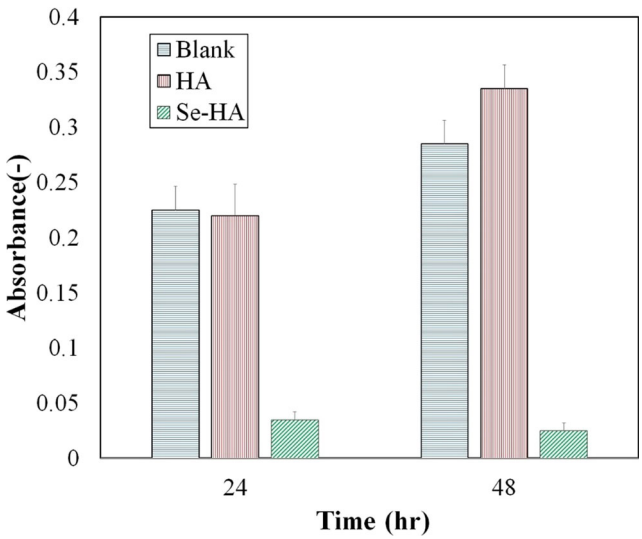

Fig. 6 MTT test for Human Bone Osteosarcoma cell line (KHOS-240S) in HA and Se-HA culture media after 24 and 48 h

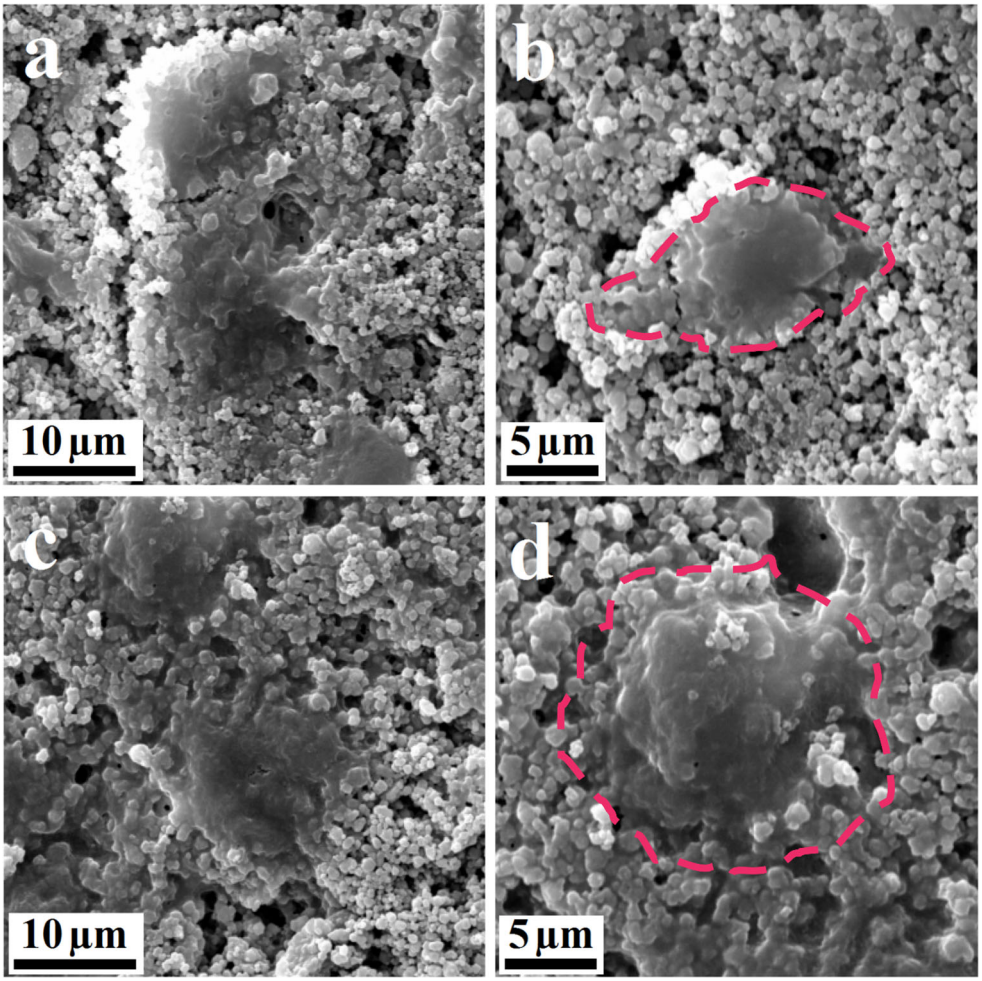

Fig. 7 SEM micrographs of the cross section of hAD-MSCs with HA (**a**, **b**) and Se-HA (**c**, **d**) scaffolds on day 3

SEM/EDX Characterization

A combined SEM/EDX instrument was applied as a tool to characterize the morphology, particle size, and elemental composition of samples. Figure 2 illustrates the SEM micrographs of HA and Se-HA samples accompanied by EDX elemental analysis. According to the SEM analysis, the size of particles was somehow under 200 nm, and the morphology was in a multi-walled sphere-like shape. It is noticeable that the morphology of HA particles was not changed by doping of Se. Furthermore, EDX results of the Se-HA sample demonstrated Se in addition to Ca, P, and O elements.

FT-IR Characterization

The identification of functional groups was accomplished by FT-IR analysis. Figure 3 exhibits the FTIR spectrum of HA and Se-HA samples. As represented in the spectra, bonds of phosphates, carbonates, and hydroxyl groups are recognizable in HA and Se-HA samples. Compared to the HA spectrum, the intensity of phosphate peak in Se-HA bioceramic was reduced. This observation was probably due to the substitution of phosphor atoms by selenium.

Figure 4 depicts the 3D structure of HA and Se-HA. As shown, the SeO_4^{-3} group is exchanged by PO_4^{-3}. Accordingly, in the FTIR spectrum of Se-HA, the absorption peak formed at 800 cm^{-1} may be related to the SeO_4^{-3} group.

In Vitro Cell Analysis

Assessment of Cell Viability

Cell viability measurement based on metabolic activity is an important assessment for cell-based applications. In the present study, cell proliferation phenomena were investigated on the Se dopant using hAD-MSCs and Human Bone Osteosarcoma cell line (KHOS-240S). Figure 5a shows the results of MTT test on hAD-MSCs after 3, 5, and 7 days of culture. As seen, the presence of Se in the HA structure had an additive effect on the proliferation of MSC cells. Moreover, there was almost the amount of 30% rise in cell expansion in the Se-HA samples after 7 days compared to the HA. It seems that Se exerts a synergistic proliferative effect on the cells

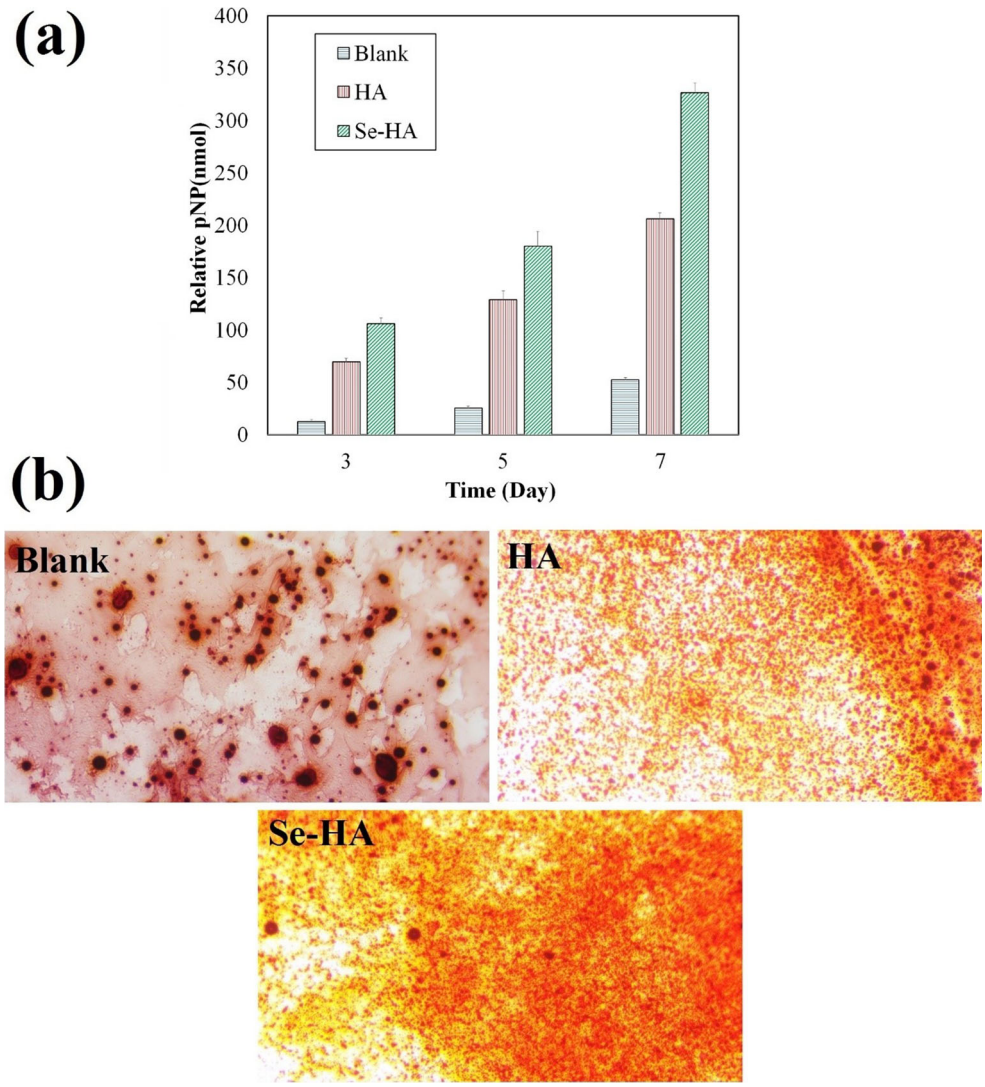

Fig. 8 **a** Alkaline phosphatase activity of hAD-MSCs in HA and Se-HA culture media on days 3, 5, and 7. **b** Alizarin red S staining of cells on the HA and Se-HA scaffolds on day 7

through enhanced Ca^{2+} ions on the Se-HA scaffold. The presence of selenite ions in the HA structure increases the absorption of Ca^{2+} ions on the surface due to a lower isoelectric point (IEP) of selenite which is 5.5. It is noticeable that the IEP of HA is 6.5 without any dopant [24]. The intensity of Ca^{2+} ions affects cell growth on the surface of bioceramic via the improvement of cell-substrate interactions [25].

Additionally, the anticancer activity of engineered Se-HA scaffold was examined using a Human Bone Osteosarcoma cell line (KHOS-240S). In comparison with the control group, cell proliferation was predominantly suppressed on the Se dopant, whereas it was promoted on the HA after 48 h of incubation (Fig. 6). This finding is consistent with previous studies, reflecting the anti-bone cancer property of Se-HA bioceramic [13, 14].

According to the results of the present study, the Se dopant has a selective cytotoxic effect on the hAD-MSCs and Human Bone Osteosarcoma cell line (KHOS-240S). This dual activity makes Se-HA scaffold a potential candidate for use in osteosarcoma defects.

Assessment of Cell Adhesion Behavior

Figure 5b displays the optical microscopy images of culture media intersection with HA and Se-HA samples after 7 days. As it is clear, the intersection of culture media with Se-HA had a more accumulative cell in comparison with the other one. Furthermore, the MSCs appear to be differentiated into osteoblast cells according to the morphology of cells contacted with the Se-HA sample.

The following figure shows SEM micrographs of the cross section of hAD-MSCs with HA (Fig. 7a, b) and Se-HA (Fig. 7c, d) scaffolds after 3 days. Obviously, the accumulation of cells on the Se-HA sample was more than HA. Increased cell adhesion on the surface of bone scaffold leads to more cell proliferation, confirming the results of MTT method. The interaction between cells and the surface of a bioceramic depends on the chemistry of surface [26]. The selenite-induced adsorption of Ca^{2+} ions on the Se-HA can promote cell adhesion by improving the function of cell-adhesive molecules

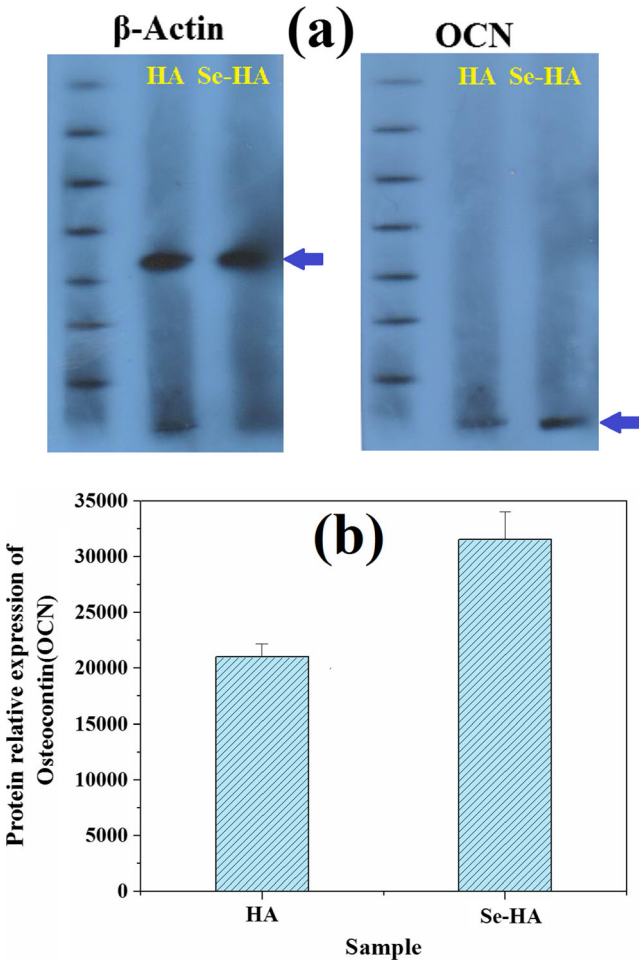

Fig. 9. **a** Western blot tests for osteocalcin (OCN) and Beta-actin proteins in hAD-MSCs. **b** Quantity evaluation of OCN protein on day 7

located on the cell surfaces [25]. So therefore, cells display more cell affinity for Se dopant.

Assessment of ALP Activity

In the process of MSCs differentiation into osteoblast, various gens including osteopontin, osteocalcine, osteonektin, remix 2, collagen type 1, and alkaline phosphatase play roles [27, 28]. Usually, ALP regards as the most important regulatory gene-promoting osteogenesis [27, 28]. Figure 8a depicts the curve related to the ALP activity of cells on the HA and Se-HA scaffolds in comparison with the scaffold-free group. Clearly, there is a meaningful difference between the activities of ALP on the surface of HA and Se-HA samples after incubation for 3, 5, and 7 days. Furthermore, the ALP activity showed an ascending trend over 7 days. As shown, the activity of ALP was elevated (> 50%) with Se addition into HA which was a reason for osteogenesis promotion. The results were in line with the results obtained by Dan Meng et al. According to their findings, increasing concentration of Ca^{2+} ions on the surface of scaffolds results in enhanced ALP activity in cells [25].

Assessment of calcification

ARS staining was conducted to determine the amount of calcium deposition in hAD-MSCs. Figure 8b presents the microscopic images of MSCs after coloring with ARS in the cell culture media including HA, Se-HA, and control samples. ARS, as an organic compound, makes the inorganic matrix of calcium change to red. If the surface is red after using ARS, it means that the surface is full of calcium. Regarding the images, the intensity of red color was raised by the doping of Se in HA which was a reason for more existence of calcium compounds on the surface.

Assessment of protein expression

Western blot is a technique used to identify and quantify the expression of target proteins. Figure 9a shows the results of Western blot tests for osteocalcin (OCN) and Beta-actin proteins. Figure 9b reveals the quantity of OCN protein. As illustrated, the amount of OCN protein in Se-HA culture media was 1.5 times greater than the amount of protein in HA culture media. Osteocalcin modulates the osteogenic differentiation of MSCs and presents as a late marker for bone formation. Accordingly, the existence of Se in the structure of HA increases the osteogenesis properties of bioceramic up to 50%. Based on the findings of previous studies, it seems that Se induces osteoblast cell differentiation by the regulation of reactive oxygen species (ROS) status [29].

Conclusion

In the present investigation, the effect of Se dopant on osteogenesis properties of HA bioceramic was studied. The presence of Se in the microstructure of HA synergistically increased the proliferation of hAD-MSCs (> 30%) after 7 days. Additionally, excellent cell adhesion and osteoblast-shaped behaviors were found on the Se dopant. The investigation of osteogenesis by the ALP test showed increased ALP activity (> 50%) on the Se-HA bioceramic. Likewise, the results of ARS staining demonstrated the additive effect of Se on the calcium deposition in hAD-MSCs. Moreover, the expression of OCN protein in the Se-HA cell culture was upregulated 1.5-fold over HA cell culture. Further investigation using Human Bone Osteosarcoma cell line (KHOS-240S) revealed anti-bone cancer property of the Se dopant, indicating its potential usability as a bifunctional scaffold for simultaneous tumor therapy and bone regeneration.

Funding Information The study was supported by Elite Researcher Grant Committee under award number (No. 982951) from the National Institutes for Medical Research Development (NIMAD), Tehran, Iran.

Compliance with Ethical Standards

Conflict of Interest The authors declare that they have no conflict of interest.

References

1. Woodard JR, Hilldore AJ, Lan SK, Park CJ, Morgan AW, Eurell JAC, Clark SG, Wheeler MB, Jamison RD, Johnson AJW (2007) The mechanical properties and osteoconductivity of hydroxyapatite bone scaffolds with multi-scale porosity. Biomaterials 28(1):45–54. https://www.sciencedirect.com/science/article/pii/S014296120600723X
2. Danilchenko SN, Kalinkevich OV, Pogorelov MV, Kalinkevich AN, Sklyar AM, Kalinichenko TG, Ilyashenko VY, Starikov VV, Bumeyster VI, Sikora VZ, Sukhodub LF (2011) Characterization and in vivo evaluation of chitosan-hydroxyapatite bone scaffolds made by one step coprecipitation method. J Biomed Mater Res A 96(4):639–647. https://europepmc.org/article/med/21268238
3. Liu Z, Liang H, Shi T, Xie D, Chen R, Han X, Shen L, Wang C, Tian Z (2019) Additive manufacturing of hydroxyapatite bone scaffolds via digital light processing and in vitro compatibility. Ceram Int 45(8):11079–11086. https://www.sciencedirect.com/science/article/pii/S0272884219304961
4. Scalera F, Palazzo B, Barca A, Gervaso F (2020) Sintering of magnesium-strontium doped hydroxyapatite nanocrystals: towards the production of 3D biomimetic bone scaffolds. J Biomed Mater Res A 108(3):633–644. https://doi.org/10.1002/jbm.a.36843
5. Ge M, Ge K, Gao F, Yan W, Liu H, Xue L, Jin Y, Ma H, Zhang J (2018) Biomimetic mineralized strontium-doped hydroxyapatite on porous poly (l-lactic acid) scaffolds for bone defect repair. Int J Nanomed 13:1707. https://www.ncbi.nlm.nih.gov/pubmed/29599615
6. Vila M, García A, Girotti A, Alonso M, Rodríguez-Cabello JC, González-Vázquez A, Planell JA, Engel E, Buján J, García-Honduvilla N, Vallet-Regí M (2016) 3D silicon doped hydroxyapatite scaffolds decorated with Elastin-like Recombinamers for bone regenerative medicine. Acta Biomater 45:349–356. https://www.sciencedirect.com/science/article/abs/pii/S1742706116304792
7. Xie H, Wang Q, Ye Q, Wan C, Li L (2012) Application of K/Sr co-doped calcium polyphosphate bioceramic as scaffolds for bone substitutes. J Mater Sci Mater Med 23(4):1033–1044. https://link.springer.com/article/10.1007/s10856-012-4556-z
8. Wang Y, Yang X, Gu Z, Qin H, Li L, Liu J, Yu X (2016) In vitro study on the degradation of lithium-doped hydroxyapatite for bone tissue engineering scaffold. Mater Sci Eng C 66:185–192. https://www.sciencedirect.com/science/article/abs/pii/S0928493116303721
9. Ofudje EA, Adeogun AI, Idowu MA, Kareem SO (2019) Synthesis and characterization of Zn-Doped hydroxyapatite: scaffold application, antibacterial and bioactivity studies. Heliyon 5(5):e01716. https://www.sciencedirect.com/science/article/abs/pii/S2405844016303721
10. Dubnika A, Loca D, Rudovica V, Parekh MB, Berzina-Cimdina L (2017) Functionalized silver doped hydroxyapatite scaffolds for controlled simultaneous silver ion and drug delivery. Ceram Int 43(4):3698–3705. https://www.sciencedirect.com/science/article/pii/S0272884216322210
11. Simon AT, Dutta D, Chattopadhyay A, Ghosh SS (2019) Copper nanocluster-doped luminescent hydroxyapatite nanoparticles for antibacterial and antibiofilm applications. ACS Omega 4(3):4697–4706. https://doi.org/10.1021/acsomega.8b03076
12. Rodríguez-Valencia C, López-Álvarez M, Cochón-Cores B, Pereiro I, Serra J, Gonzalez P (2013) Novel selenium-doped hydroxyapatite coatings for biomedical applications. J Biomed Mater Res A 101(3):853–861. https://onlinelibrary.wiley.com/doi/abs/10.1002/jbm.a.34387
13. Khan S, Ullah MW, Siddique R, Liu Y, Ullah I, Yang G, Xue M, Hou H (2019) Catechins-modified selenium-doped hydroxyapatite nanomaterials for improved osteosarcoma therapy through generation of reactive oxygen species. Front Oncol 9:499. https://www.frontiersin.org/articles/10.3389/fonc.2019.00499/full
14. Zhou ZF, Sun TW, Qin YH, Zhu YJ, Jiang YY, Zhang Y, Liu JJ, Wu J, He SS, Chen F (2019) Selenium-doped hydroxyapatite biopapers with an anti-bone tumor effect by inducing apoptosis. Biomater Sci 7(12):5044–5053. https://pubs.rsc.org/en/content/articlelanding/2019/bm/c9bm00953a#!divAbstract
15. Wang J, Xue C, Zhu P (2017) Hydrothermal synthesis and structure characterization of flower-like self assembly of silicon-doped hydroxyapatite. Mater Lett 196:400–402. https://www.sciencedirect.com/science/article/abs/pii/S0167577X17303981
16. Pham VH, Van HN, Tam PD, Ha HNT (2016) A novel 1540 nm light emission from erbium doped hydroxyapatite/β-tricalcium phosphate through co-precipitation method. Mater Lett 167:145–147. https://www.sciencedirect.com/science/article/abs/pii/S0167577X16300027
17. Iqbal N, Kadir MRA, Malek NANN, Mahmood NH, Murali MR, Kamarul T (2012) Rapid microwave assisted synthesis and characterization of nanosized silver-doped hydroxyapatite with antibacterial properties. Mater Lett 89:118–122. https://www.sciencedirect.com/science/article/abs/pii/S0167577X12011767
18. He W, Xie Y, Xing Q, Ni P, Han Y, Dai H (2017) Sol-gel synthesis of biocompatible Eu3+/Gd3+ co-doped calcium phosphate nanocrystals for cell bioimaging. J Lumin 192:902–909. https://www.sciencedirect.com/science/article/abs/pii/S0022231317306154
19. Guanzhou YHQ, Dianzuo W (2001) Mechano-chemical synthesizing of specially functional powder. Met Miner 1:7. http://en.cnki.com.cn/Article_en/CJFDTotal-JSKS200101007.htm
20. Mucsi G (2019) A review on mechanical activation and mechanical alloying in stirred media mill. Chem Eng Res Des 148:460–474. https://www.sciencedirect.com/science/article/abs/pii/S0263876219303119
21. Alkaline phosphatase FS (DGKC). shorturl.at/cep19, 2016 (844 0401 10 02 00)
22. Monshi A, Foroughi MR, Monshi MR (2012) Modified Scherrer equation to estimate more accurately nano-crystallite size using XRD. World J Nano Sci Eng 2(3):154–160. https://m.scirp.org/papers/23195
23. Wei L, Pang D, He L, Deng C (2017) Crystal structure analysis of selenium-doped hydroxyapatite samples and their thermal stability. Ceram Int 43(18):16141–16148. https://www.sciencedirect.com/science/article/pii/S0272884217319028
24. Maleki-Ghaleh H, Aghaie E, Nadernezhad A, Zargarzadeh M, Khakzad A, Shakeri MS, Khosrowshahi YB, Siadati MH (2016) Influence of Fe_3O_4 nanoparticles in hydroxyapatite scaffolds on proliferation of primary human fibroblast cells. J Mater Eng Perform 25(6):2331–2339. https://doi.org/10.1007/s11665-016-2086-4
25. Meng D, Dong L, Yuan Y, Jiang Q (2019) In vitro and in vivo analysis of the biocompatibility of two novel and injectable calcium phosphate cements. Regen Biomater 6(1):13–19. https://academic.oup.com/rb/article/6/1/13/5253839

26. John AA, Subramanian AP, Vellayappan MV, Balaji A, Jaganathan SK, Mohandas H, Paramalinggam T, Supriyanto E, Yusof M (2015) physico-chemical modification as a versatile strategy for the biocompatibility enhancement of biomaterials. RSC Adv 5(49):39232–39244. https://pubs.rsc.org/en/content/articlelanding/2015/ra/c5ra03018h#!divAbstract
27. Carroll SH, Ravid K (2013) Differentiation of mesenchymal stem cells to osteoblasts and chondrocytes: a focus on adenosine receptors. Exp Rev Mol Med 15. https://www.ncbi.nlm.nih.gov/pubmed/23406574
28. Valenti MT, Dalle CL, Donatelli L, Bertoldo F, Zanatta M, Cascio VL (2008) Gene expression analysis in osteoblastic differentiation from peripheral blood mesenchymal stem cells. Bone 43(6):1084–1092. https://www.sciencedirect.com/science/article/abs/pii/S8756328208006005
29. Huawei Z, Jay JC, Gerald FC (2013) Selenium in bone health: roles in antioxidant protection and cell proliferation. Nutrients 5(1):97–100. https://www.mdpi.com/2072-6643/5/1/97